Ultrahigh energy cosmic ray nuclei from remnants of dead quasars

Roberto J. Moncada,[1,2] Rafael A. Colon,[1,3] Juan J. Guerra,[1,3] Matthew J. O'Dowd,[1,3,4] and Luis A. Anchordoqui[1,3,4]

[1]*Department of Astrophysics, American Museum of Natural History, Central Park West 79 St., NY 10024, USA*
[2]*Department of Physics, City College, City University of New York, NY 10031, USA*
[3]*Department of Physics and Astronomy, Lehman College, City University of New York, NY 10468, USA*
[4]*Department of Physics, Graduate Center, City University of New York, 365 Fifth Avenue, NY 10016, USA*
(Dated: January 2017)

We re-examine the possibility of ultrahigh energy cosmic rays being accelerated in nearby dormant quasars. We particularize our study to heavy nuclei to accommodate the spectrum and nuclear composition recently reported by the Pierre Auger Collaboration. Particle acceleration is driven by the Blandford-Znajek mechanism, which wires the dormant spinning black holes as Faraday unipolar dynamos. We demonstrate that energy losses are dominated by photonuclear interactions on the ambient photon fields. We argue that the local dark fossils of the past quasar activity can be classified on the basis of how source parameters (mass of the central engine and photon background surrounding the accelerator) impact the photonuclear interaction. In this classification it is possible to distinguish two unequivocal type of sources: those in which nuclei are completely photodisintegrated before escaping the acceleration region and those in which photopion production is the major energy damping mechanism. We further argue that the secondary nucleons from the photodisintegrated nuclei (which have a steep spectral index at injection) can populate the energy region below "the ankle" feature in the cosmic ray spectrum, whereas heavy and medium mass nuclei (with a harder spectral index) populate the energy region beyond "the ankle", all the way to the high energy end of the spectrum. In addition, we show that five potential quasar remnants from our cosmic backyard correlate with the hot-spot observed by the Telescope Array.

I. INTRODUCTION

The origin(s) of ultrahigh energy cosmic rays (UHECRs) remains a central question in high energy astrophysics [1, 2]. Three principle observables drive the search for and characterization of cosmic ray sources: the energy spectrum, the nuclear composition, and the distribution of arrival directions. The cosmic ray energy spectrum encompasses a plummeting flux that drops from $10^4 \; \mathrm{m^{-2} \, s^{-1}}$ at $E \sim 1$ GeV to $10^{-2} \; \mathrm{km^{-2} \, yr^{-1}}$ at $E \sim 10^{11}$ GeV. Its shape is remarkably featureless and can be described by a broken power law: the spectrum steepens gradually from $E^{-2.7}$ to $E^{-3.3}$, then flattens to $E^{-2.6}$ near $10^{9.6}$ GeV forming a feature known as "the ankle", and drops sharply at around $10^{10.5}$ GeV [3–5]. The small variations of the spectral index can be interpreted either as a transition between cosmic ray populations, or as an imprint of cosmic ray propagation effects.

The simplest interpretation of the ankle is that above $10^{9.6}$ GeV a new population emerges which dominates the more steeply falling Galactic population of heavy nuclei. The extragalactic component can be dominated either by protons [6] or heavies [7, 8]. Proton-dominance beyond the ankle is ultimately limited by the onset of photopion production on the cosmic microwave background, whereas dominance of a heavy composition is restricted by nucleus photodisintegration through the giant dipole resonance – the so called *Greisen-Zatsepin-Kuz'min* (GZK) suppression at around $10^{10.5}$ GeV [9, 10]. It has also been advocated that the ankle feature could be well reproduced by a proton-dominated power-law spectrum, where the ankle is formed as a *dip* in the spectrum from the energy loss of protons via Bethe-Heitler pair production [11, 12]. In this case extra-galactic protons would already have started to dominate the spectrum somewhat beyond $10^{8.7}$ GeV.

Optical observations of air showers with fluorescence telescopes or non-imaging Cherenkov detectors consistently find a predominantly light composition at around 10^9 GeV [13] and the contribution of protons to the overall cosmic ray flux is $\gtrsim 50\%$ in this energy range [14–17]. Due the absence of a large anisotropy in the arrival direction of cosmic rays below the ankle [18, 19], we can conclude that these protons must be of extra-galactic origin. At energies above 10^{10} GeV, the high-statistics data from the Pierre Auger Observatory suggests a gradual increase of the fraction of heavy nuclei in the cosmic ray flux [14–17]. Within uncertainties, the data from the Telescope Array (TA) is consistent with these findings [20, 21]. Moreover, the Telescope Array has observed a statistically significant excess in cosmic rays with energies above $10^{10.7}$ GeV in a region of approximately 1150 square degrees centered on equatorial coordinates (R.A. = 146.7°, Dec. = 43.2°) – the TA hot spot [22]. The absence of a concentration of nearby sources in this region of the sky favors a heavy nucleus hypothesis, whereby a few local sources within the GZK sphere can produce the hot spot through deflection in the Galactic **B**-field. All in all, the apparent dominance of heavy nuclei in the vicinity of 10^{10} GeV strongly argues against the interpretations of the ankle given above.

One can (of course) accommodate the data with the addition of an *ad hoc* light extragalactic component below the ankle, with a steep injection spectrum [23]. However, a more natural explanation of the entire spectrum and composition emerges while accounting for the "post-processing" of UHECRs through photodisintegration in the environment surrounding the source [24–27]. In such models relativistic nuclei accelerated by a central engine to extremely high energies remain trapped in the turbulent magnetic field of the source environment. Their escape time decreases faster than the interaction time with increasing energy, so that only the highest energy nuclei can escape the source unscathed. In effect, the source environment acts as a high-pass filter on the spec-

trum of cosmic rays. All nuclei below the energy filter interact, scattering off the far-infrared photons in the source environment. These photonuclear interactions produce a steep spectrum of secondary nucleons, which is overtaken by the harder spectrum of the surviving nucleus fragments above about $10^{9.6}$ GeV. These overlapping spectra could then carve an ankle-like feature into the source emission spectrum. The spectrum above the ankle exhibits a progressive transition to heavy nuclei, as the escape of non-interacting nuclei becomes efficient. In such models, the source evolution with redshift plays a paramount role on the source parameters. For models with positive redshift evolution (a greater number of sources per comoving volume at high redshift), both the imposition of a dominant light extragalactic component below the ankle and the source-ankle model favor a hard injection spectrum $\propto E^{-1}$. However, it has been recently noted that fitting the high end of the cosmic ray (CR) spectrum and composition with negative source evolution allows for softer injection spectra [28].

On a separate track, it was recently pointed out that Fermi-LAT observations [29, 30] severely constrain the distribution of UHECR sources [31]. This is because on the way to Earth UHECRs interact with the radiation fields permeating the universe and give rise to energetic electron/positron pairs and photons, which in turn feed electromagnetic cascades resulting in a diffuse gamma-ray background radiation. The recent study in [31] suggests that a local "fog" of UHECRs accelerated in nearby sources must exist so as to not overproduce the cascade gamma-ray flux beyond Fermi-LAT observations.

In consideration of these new results, it seems interesting to explore whether remnants of dead quasars, which are distributed preferentially in the low-redshift universe, could accelerate heavy nuclei up to the highest observed energies. Actually, nearby quasar remnants have long been suspected to be sources of UHECRs [32–35]. Particle acceleration proceeds via the Blandford-Znajek mechanism, which wires dormant spinning black holes as Faraday unipolar dynamos [36, 37]. Detailed modeling with reasonable assumptions on source parameters suggests that protons can be efficiently launched at $E \gtrsim 10^{12}$ GeV. Photopion production in collisions with ambient photons becomes a relatively important effect during the final phase of the acceleration process, and could damp the maximum attainable energy to values well below that imposed by the voltage drop. The large charge Ze of heavy nuclei facilitates their acceleration to highest energy (scaling linearly with Z). However, heavy nuclei could also interact with the ambient photons and may suffer significant spallation. In this paper we study in detail the dominant processes for nucleus energy losses, while searching for plausible source parameters which may allow acceleration of heavy nuclei up to the highest observed energies.

The layout of the paper is as follows. In Sec. II we provide an assessment of what is known observationally about the evolution of quasar activity and then discuss the general framework use to relate the quasar population with massive dark objects at the center of local inactive galaxies. We also show that five nearby relics of such past activity correlate with the TA hot-spot. In Sec. III we review the generalities of particle acceleration near the event horizon of a spinning supermassive black hole and determine plausible source conditions for acceleration of UHECR nuclei. In Sec. IV we examine the various energy-loss mechanisms of one-shot acceleration, including radiative processes and photonuclear interactions with the ambient photons. We show that, in general, photonuclear energy losses are dominant. After that we propose a novel phenomenological model to explain the evolution of the UHECR spectrum and composition with energy, without fine-tuning. Finally, in Sec. V we present our conclusions.

II. DORMANT BLACK HOLES AFTER A SHINING PAST

The first extensive radio surveys of the 1950s revealed a new family of radio sources that, by the early 60s, had been associated with point-like optical counterparts [38]. These quasi-stellar radio sources, or quasars, revealed very large systemic redshifts indicating cosmological distances [39]. This implied luminosities up to hundreds of times that of the Milky Way, apparently emitted from very small size-scales [40], suggesting an extremely energetic emission mechanism. It has now been established that quasars are ultimately powered by the accretion of matter onto the $10^7 - 10^{10} M_\odot$ supermassive black holes (SMBHs) at cores of galaxies [41–45].

Quasars and their relativistically-beamed counterparts, blazars, are the most luminous sub-class of *active galactic nuclei* (AGNs), which is the general name for an actively-accreting SMBH. In fact, these objects are the most luminous continuously-emitting objects in the Universe. Quasar luminosity is, to first order, constrained by the Eddington limit [46]. This is the maximum luminosity of a spherically accreting object, determined by the point at which outward radiation pressure halts gravitational infall. The Eddington limit is proportional to the mass of the accreting object. Scaled for a quasar powered by a SMBH of $10^9 M_\odot$, this luminosity is:

$$L_{\rm Edd} = 1.3 \times 10^{47} \frac{M}{10^9 M_\odot} \text{ erg/s} \sim 10^2 L_{\rm galaxy} , \qquad (1)$$

where $M_\odot$ is the solar mass and $L_{\rm galaxy}$ is the bolometric luminosity of large galaxies like the Milky Way. Note that accretion by the standard α-disk, which is typically assumed for quasars, is also Eddington limited [47].

It is generally accepted that the number density of quasars peaked at redshift $z \sim 2$, when the universe was one-fifth of its present age [48]. Locally, essentially all galaxies with spheroidal components contain a SMBH [49–51]. The close relationships between the masses of these SMBHs and their host galaxy's properties, including stellar velocity dispersion, spheroidal luminosity, and dynamical mass, indicates that the growth of SMBHs and their hosts are closely tied [52–56]. These relationships also allow us to make a relatively direct determination of the local SMBH mass function [57–61].

Another approach to deriving the local SMBH mass function is to integrate SMBH accretion over cosmic time based on the evolving high-z quasar luminosity function [60–67]. Such models are able to reproduce the "observed" low-z mass function for quiescent SMBHs very successfully by assuming the typical radiative efficiencies for an α-disk ($0.1 \lesssim \eta \lesssim 0.2$),

and reasonable Eddington fractions — quasar luminosities as a fraction of the Eddington limit (Eddington fraction) — of $0.2 \lesssim L/L_{Edd} \lesssim 1$ [59, 60, 65, 66, 68]. This general agreement supports for the idea that accretion in AGN mode is an important, and perhaps the principle mechanism by which local SMBHs grow [48, 60, 64, 65]. Thus, it is reasonable to assume that many of the more massive quiescent SMBHs in the local universe are "remnant" quasars [48, 63], and that these greatly outnumber active quasars in the modern epoch.

In their active phases, accreting SMBHs are expected to support strong magnetic fields. Assuming a rapidly-rotating black hole, which may be common in luminous quasars [65, 69], this magnetic field is expected to survive the expiration of the quasar phase. We calculate a typical relic magnetic field strength for a rapidly rotating SMBH by assuming that it corresponds to maximum field strength acquired during its quasar phase. This in turn corresponds to its maximum accretion rate. To determine this accretion rate we assume the lower end of α-disk radiative efficiency, $\eta = 0.1$ (corresponding to a higher accretion rate per unit luminosity), and that the quasar radiates at the Eddington limit. The mass accretion rate needed to sustain the Eddington luminosity is

$$\dot{M}_{Edd} = \frac{L_{Edd}}{\eta c^2} \simeq 22 \, M_9 \, M_\odot \, \text{yr}^{-1} \,. \tag{2}$$

where $M_9 = M/(10^9 M_\odot)$. The accreting plasma is assumed to support an axisymmetric magnetic field configuration due to the generation of currents. Following [32], we get an estimate of the characteristic magnetic field strength B_0 by assuming pressure equilibrium between the magnetic field and the in-falling matter [70]

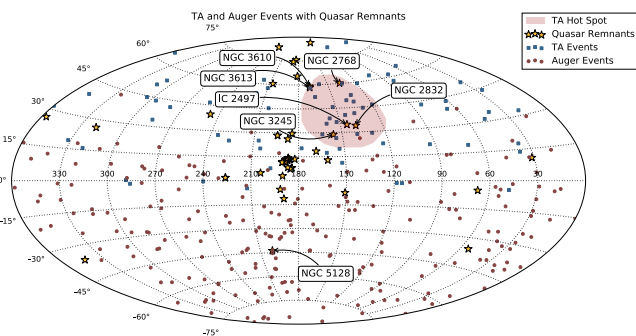$$B_0 \sim 10^4 \, M_9^{-1/2} \left(\frac{\dot{M}}{\dot{M}_{Edd}} \right)^{1/2} \text{G} \,. \tag{3}$$

FIG. 1. Comparison of UHECR event locations with quasar remnants in equatorial coordinates, with R.A. increasing from right to left. The circles indicate the arrival directions of 231 events with $E > 52$ EeV and zenith angle $\theta < 80°$ detected by the Pierre Auger Observatory from 2004 January 1 up to 2014 March 31 [83–86]. The squares indicate the arrival directions of 72 events with $E > 57$ EeV and $\theta < 55°$ recorded from 2008 May 11 to 2013 May 4 with TA [22]. The stars indicate the location of nearby quasar remnants [34, 87]. The shaded region delimits the TA hot-spot. The locations of the sources inside the TA hot-spot and the closest object in the survey (NGC 5128) are explicitly identified.

This magnetic field may be taken as a fiducial strength for quasars remnants at the upper end of the local SMBH mass and spin functions.

This represents the magnetic field strength developed by a maximally rotating black hole at the peak of its accretion phase and at the upper end of the mass function. In the following calculations we work with this fiducial strength, yielding. It will be seen that a relatively high field strength, $B_0 \sim 10^4$ G, is necessary to achieve a significant flux of 10^{11} GeV single-proton CRs around a $10^9 \, M_\odot$ SMBH. However, when we consider black holes up to $10^{10} \, M_\odot$, and heavy nuclei CRs, the required field strength drops by up to two orders of magnitude. We also assume that a significant fraction of the maximum field strength is sustained as accretion rate drops into the remnant quasar phase. Further data on the spatial association of UHECRs with SMBHs will test this assumption.

Significant magnetic fields do appear to survive in the case of least one class of remnant quasar. BL Lacertae objects are AGNs of the blazar class – broadly, AGNs with jets that are closely aligned with our line of sight [45, 71]. BL Lacs show little or no signs of broad emission lines or thermal emission [45, 72, 73]. This implies that at least a subset of BL Lacs are starved of gas, and perhaps in a post-quasar phase. Under this interpretation, flat-spectrum radio quasars (FSRQs) become the progenitor population of low-accretion BL Lacs [74–76]. This evolutionary argument is supported by BL Lacs' negative cosmological evolution; their number densities rise at around the same epoch as the decline of FS-RQs [77]. BL Lacs exhibit BZ-powered jets [78], indicating that significant magnetic fields may be sustained long after the cessation of significant accretion.

Hanny's Voorwerp contains perhaps the first direct probe of quasar evolution [79]. Observations in the optical, ultra-violet, and X-ray indicate that this unusual object near the spiral galaxy IC 2497 contains highly ionized gas [80]. The emission-line properties, and lack of X-ray emission from IC 2497, seem to indicate this spiral galaxy is a highly obscured AGN with a novel geometry arranged to allow photoionization of Hanny's Voorwerp but not the galaxy's own circumnuclear gas [81], or alternatively the luminosity of the central source has decreased dramatically within the last 10^5 yr [82]. Should this be the case, Hanny's Voorwerp may exemplify the first detection of a quasar light echo. Interestingly, IC 2497 is inside the TA hot spot; see Fig. 1. However, the measured redshift $z = 0.05$ of IC 2497, sets this dormant quasar outside our local GZK–horizon (~ 100 Mpc). To sample sources inside the GZK–sphere we adopt a distance-limited ($z \lesssim 0.02$) compilation of quasar remnant candidates, capable of accelerating UHECRs [34, 87]. It is compelling that five of the objects contained in this sample are also inside the TA hot spot; see Fig. 1.

Centaurus A (Cen A) is a complex radio-loud source identified at optical frequencies with the galaxy NGC 5128. Cen A is the closest radiogalaxy to Earth (distance ~ 3.4 Mpc) and has long been suspected to be a potential UHECR accelerator [88, 89]. The Pierre Auger Collaboration has searched for anisotropies in the direction of Cen A scanning the energy threshold between $10^{10.6}$ GeV and $10^{10.9}$ GeV and count-

ing events in angular radii ranging from 1° to 30° [83]. The strongest departure from isotropy (post-trial probability $\sim 1.4\%$) has been observed for $E > 58$ EeV in a window of 15°: 14 events (out of a total of 155) have been observed in such an angular window while 4.5 are expected on average from isotropic distributions.

A statistical analysis to ascertain the significance of a possible correlation between UHECRs and SMBHs would require using data from Auger and TA. However, if the high energy end of the cosmic ray spectrum is the same in the north and in the south, there appears to be a difference in the energy scale between the two detectors [90], making such study unreliable at present. Future experiments that will observe both hemispheres using the same apparatus, such as the Probe Of Extreme Multi-Messenger Astrophysics (POEMMA), would make a robust statistical analysis more straightforward.[1]

For convenience, we subdivide the SMBH sample into two subcomponents: one with masses $\gtrsim 10^{10} M_\odot$ and one with masses $\lesssim 10^{10} M_\odot$. The rationale for using $10^{10} M_\odot$ as the demarcation mass will become evident in Sec. IV. Roughly speaking, 16% of SMBHs have mass above $10^{10} M_\odot$ [87]. Inside the TA hot spot one of six (five nearby) candidate sources is consistent with a mass $\gtrsim 10^{10} M_\odot$. Thus, we can assume that the ratios inside the hot spot are representative of the ratios of the universe at large.

III.   UHECR ACCELERATION IN QUASAR REMNANTS

In realistic astrophysical situations involving quasars, the black hole itself is uncharged, and the gravity of the accretion disk is practically negligible. This means that the geometry of spacetime is described by the Kerr metric and therefore determined by two free parameters: the black hole mass M and its angular momentum

$$|J| = a\, J_{\max} = a\, \frac{GM^2}{c}\,, \qquad (4)$$

where $0 \le a \le 1$ is the dimensionless spin parameter [92]. Before proceeding we note that for a Schwarzschild black hole, $a = 0$ [93], whereas for a maximally spinning (a.k.a. extreme Kerr) black hole, $a = 1$. As a matter of fact, the increase of the spin parameter would stop at $a \approx 0.998$ because photons emitted from the disk on retrograde paths are more likely to be captured by the hole than prograde ones, hence de-spinning the hole [94].

For static black holes, the scale characterizing the event horizon r_h is the Schwarzschild radius

$$r_S = \frac{2GM}{c^2} \simeq 3 \times 10^{14} \left(\frac{M}{10^9 M_\odot} \right) \text{cm}\,. \qquad (5)$$

For spinning black holes, the (spherical) event horizon surface is defined by

$$r_h = r_g \left(1 + \sqrt{1 - a^2} \right)\,, \qquad (6)$$

where $r_g = r_S/2$ is the gravitational radius. The ergosphere is the region described by the relation

$$r_h < r < r_{\max} = r_g \left(1 + \sqrt{1 - a^2 \cos^2 \theta} \right)\,, \qquad (7)$$

where θ is the angle to the polar axis; see e.g. [95, 96]. Inside the ergosphere (which is ellipsoidal in shape), spacetime is pulled heavily towards the direction of the black hole rotation (frame dragging), and consequently no static observer can exist because the particles must co-rotate with the hole. The black hole's angular velocity $\mathbf{\Omega}$ coincides with the angular velocity of the dragging of inertial frames at the horizon [96]

$$|\mathbf{\Omega}| = a \left(\frac{c}{2r_h} \right)\,. \qquad (8)$$

It has long been known that a rotating black hole can radiate away its available reducible energy [97, 98]. In this context Blandford and Znajek (BZ) proposed a model of electromagnetic extraction of black hole's rotational energy based on the analogy with the classical Faraday (unipolar induction) dynamo phenomenon [36, 37]. In the BZ mechanism, the magnetic field $\boldsymbol{B}$ near the horizon taps the rotational energy of the black hole and generates powerful outflows of electromagnetic (Poynting) energy. BZ argue that spacetime frame dragging induces an electric field $\boldsymbol{E}$ that is strong enough to break the vacuum and establish an electron-positron force-free magnetosphere.

The particulars of the black hole magnetosphere could be very complicated, distinctively if the poloidal magnetic field near the horizon is misaligned with the black hole rotation axis [35]. For simplicity, herein we assume that the $\boldsymbol{B}$-field is aligned with the axis of rotation. This manageable system allows a transparent analytic calculation which captures the essence of most aspects of the BZ mechanism and leads to a correct order of magnitude.

Conduction electrons within the magnetosphere undergo collisions with the orbiting atoms, and this causes them to take up the rotational motion. At each point the electrons have a net drift velocity, $\mathbf{v} = \mathbf{\Omega} \wedge \boldsymbol{r}$, where $\boldsymbol{r}$ is the position vector of the point in question relative to an origin which is chosen to lie on the magnetic axis. The conduction electrons experience a magnetic force $-e\mathbf{v} \wedge \boldsymbol{B}$, which is mainly directed towards the central axis; as a result a negative charge appears in the core of the magnet, and a positive charge on its curved outer surface. In equilibrium an electrostatic field is set up, such that the total Lorentz force on the conduction electrons is zero. Namely, $\boldsymbol{F} = -e\boldsymbol{E} - e\mathbf{v} \wedge \boldsymbol{B} = \boldsymbol{0}$, and so

$$\boldsymbol{E} = -\mathbf{v} \wedge \boldsymbol{B}\,. \qquad (9)$$

We now calculate the potential difference V corresponding to this electric field. It is straightforward to see by inspection of (9) that along the axis of rotation $\boldsymbol{E} = 0$, and therefore $V = 0$ at all points along this axis. For a maximally spinning hole, the potential drop between the central ($r = 0$) and the marginal ($r = r_{\max}$) magnetic surfaces passing through the horizon is

---

found to be

$$V = -\int \boldsymbol{E} \cdot d\boldsymbol{s} = \int_0^{r_{\max}} \Omega B_0 \, r \, dr \sim \frac{1}{4} \frac{G}{c} M B_0$$
$$\sim \frac{1}{4} \frac{6.7 \times 10^{-11}}{3 \times 10^8} \frac{1.9 \times 10^{30}}{M_\odot} M \, B_0 \; \mathrm{m^2 s^{-1}} \,, \quad (10)$$

where B_0 is the magnetic field strength. Now, recalling that 10^4 G = 1 T = 1 V s m^{-2}, we can rewrite (10) as

$$V \sim 10^{20} \, M_9 \, B_4 \; \mathrm{V} \,, \quad (11)$$

where $B_4 = B_0/10^4$ G.

Far away from the horizon, the electromagnetic field can be expressed as [99]

$$\lim_{r \to \infty} B_{\hat{r}} = B_0 \cos\theta, \qquad \lim_{r \to \infty} B_{\hat{\theta}} = -B_0 \sin\theta, \quad (12)$$

and

$$\lim_{r \to \infty} E_{\hat{r}} = -\frac{B_0 \, aM(3\cos^2\theta - 1)}{r^2}, \quad \lim_{r \to \infty} E_{\hat{\theta}} = O(r^{-4}) \,. \quad (13)$$

The electric field has a quadrupole topology, which is distinctly seen in Fig. 2. The voltage difference between the horizon and $r = \infty$ is of order V. With such a huge voltage drop along field lines, one expects that electrons roaming in the vicinity of the horizon would be accelerated to huge energies and, upon colliding with stray photons and/or positrons, produce a cascade of e^+e^- pairs. Very quickly therefore, the vacuum surrounding the black hole would be filled with a highly conducting plasma. The plasma-loaded field lines can serve as *wires* to complete a circuit between the pole and equator of the horizon. The electromotive force around this circuit is numerically comparable to (11). Thus, if a cosmic ray baryon can fully tap this potential acceleration up to extreme energies,

$$E_{\max} = ZeV \sim 10^{11} \, Z \, M_9 \, B_4 \; \mathrm{GeV} \sim 10^{11} \, Z \, M_9^{1/2} \; \mathrm{GeV} \,, \quad (14)$$

would become possible. However, the charge density in the vicinity of accreting black holes could be so high that a significant fraction of this potential would be screened and so no longer available for particle acceleration. Therefore, it seems more appropriate to define an effective potential where the available length scale, the gap height ζ, is explicitly taken into account. Following [96], we take

$$V_{\mathrm{eff}} \sim V \left(\frac{\zeta}{r_h}\right)^2 \,. \quad (15)$$

Accordingly, the characteristic rate of energy gain is found to be

$$\left. \frac{dE}{dt} \right|_{\mathrm{acc}} = Ze \, V_{\mathrm{eff}} \, \frac{c}{\zeta} \,, \quad (16)$$

and so the acceleration timescale is given by

$$\tau_{\mathrm{acc}} = E \left[\left. \frac{dE}{dt} \right|_{\mathrm{acc}} \right]^{-1} = \frac{E}{ZeV_{\mathrm{eff}}} \frac{\zeta}{c} \,. \quad (17)$$
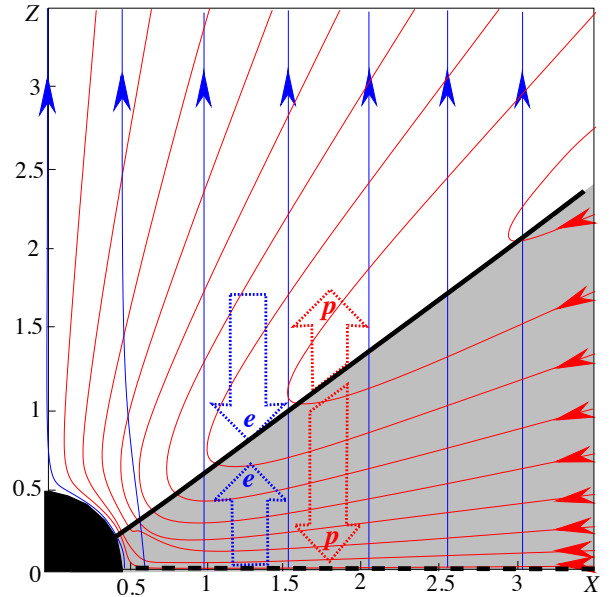

FIG. 2. Magnetic (blue solid) and electric (red solid) field lines associated to the asymptotically homogeneous $\boldsymbol{B}$ field aligned with the rotation axis of a maximally spinning black hole. The wide blue and red arrows show the directions of acceleration of electrons and protons in different regions. The acceleration can be avoided only if a particle resides at a surface at which the electric field is orthogonal to the magnetic field, the so-called force-free surfaces. Thick solid and dashed lines indicate the conical and equatorial force-free surfaces. The force-free surfaces separate different acceleration regions, with electric field directed along or oppositely to the magnetic field. Taken from [35].

In a realistic situation the energy losses of the accelerated particles limit the maximal energies to the values below the estimate of (14). It is this that we now turn to study. Before proceeding though, it is interesting to note that the axisymmetric stationary flow in the vicinity of the rotation-powered compact object could provide a source of ultrarelativistic nuclei with an extremely flat injection spectrum (typically $\propto E^{-1}$ [100, 101]), in good agreement with the requirements to accommodate Auger observations [17, 24]. Moreover, a steepened injection spectrum would arise quite naturally if the medium surrounding the compact object were leaky at these late ages.

IV. MECHANISMS OF ENERGY DISSIPATION

In the absence of energy losses the maximum Lorentz factor is given by

$$\gamma_{\max}^{\mathrm{acc}} \sim 10^{11} \frac{Z}{A} \, M_9 \, B_4 \left(\frac{\zeta}{r_h}\right)^2 \,, \quad (18)$$

where $E = \gamma A m_p$, with m_p the proton mass and A the nuclear baryon number. Within the potential drop, the nuclei follow the curved magnetic field lines and so emit curvature-radiation photons. The energy loss rate or total power radiated away by

TABLE I. Relevant source parameters and normalization factor n_0^β, for $\beta = -4, -5$.

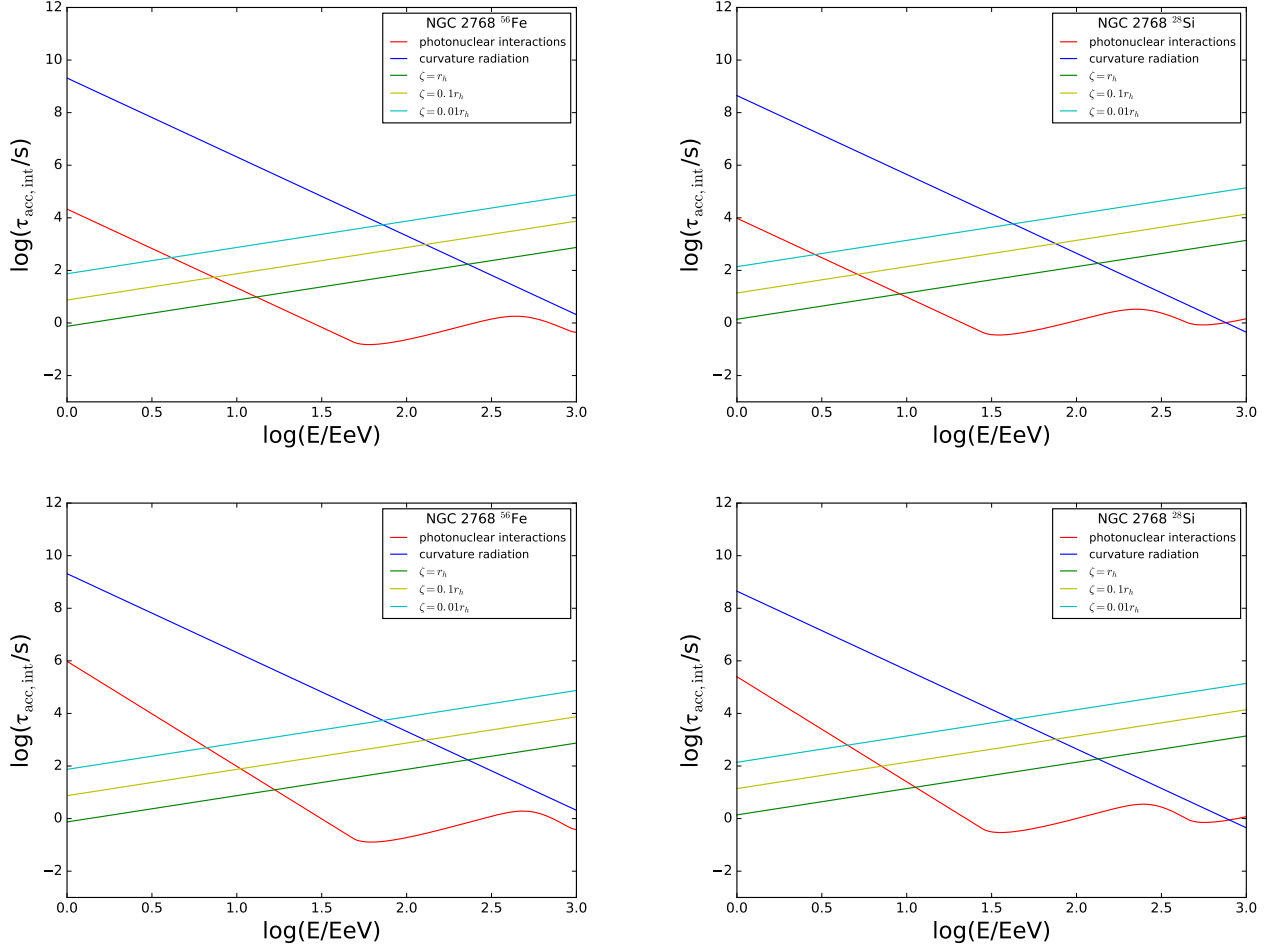| Source	$L_{\rm FIR}/L_\odot$	M_9	$n_0^{-4}/({\rm MeV\,cm^3})$	$n_0^{-5}/({\rm MeV\,cm^3})$	z	References
NGC 2768	4.8×10^8	0.16	7.8×10^{23}	1.0×10^{24}	0.0051	[34, 114, 115]
NGC 2832	$< 1.7 \times 10^8$	11.4	3.0×10^{19}	3.9×10^{19}	0.0194	[87, 115, 116]
NGC 3610	4.7×10^7	0.05	6.9×10^{23}	8.9×10^{23}	0.0066	[34, 115, 117]
NGC 3613	$< 3.6 \times 10^8$	0.16	4.8×10^{23}	6.2×10^{23}	0.0066	[34, 116, 117]
NGC 4125	3.0×10^8	0.28	1.5×10^{23}	1.9×10^{23}	0.0063	[34, 115, 117]

FIG. 3. Comparison of acceleration and interaction time scales for NGC 2768. The bumpy curve indicates the interaction time scale for photonuclear interactions. The straight line with negative slope indicate the time scale due to curvature radiation. The straight lines with positive slope correspond to acceleration time scales with different ζ. The upper panels correspond to $\beta = -4$ and the lower panels to $\beta = -5$.

a single cosmic ray is [102]

$$\frac{dE}{dt}\bigg|_{\rm loss}^{\rm rad} = \frac{2}{3}\frac{Z^2 e^2 c}{r_c^2}\gamma^4 \,, \quad (19)$$

where r_c is the curvature radius of the magnetic field lines, and γ is the Lorentz factor of the radiating particles. The characteristic cooling timescale is then given by

$$\tau_{\rm int}^{\rm rad} = \gamma A m_p \left[\frac{dE}{dt}\bigg|_{\rm loss}^{\rm rad}\right]^{-1} \,. \quad (20)$$

Acceleration gains are balanced by radiative losses. In the absence of other damping mechanisms, the radiation reaction limit is [103, 104]

$$\gamma_{\rm max}^{\rm rad} \sim 10^{11}\left(\frac{B_4}{Z}\right)^{1/4} M_9^{1/2}\left(\frac{r_c}{r_h}\right)^{1/2}\left(\frac{\zeta}{r_h}\right)^{1/4} \,. \quad (21)$$

All in all, direct electric field acceleration on the black hole magnetosphere would allow Lorentz factors up to

$$\gamma_{\rm max} = \min\left\{\gamma_{\rm max}^{\rm acc},\, \gamma_{\rm max}^{\rm rad}\right\} \,. \quad (22)$$
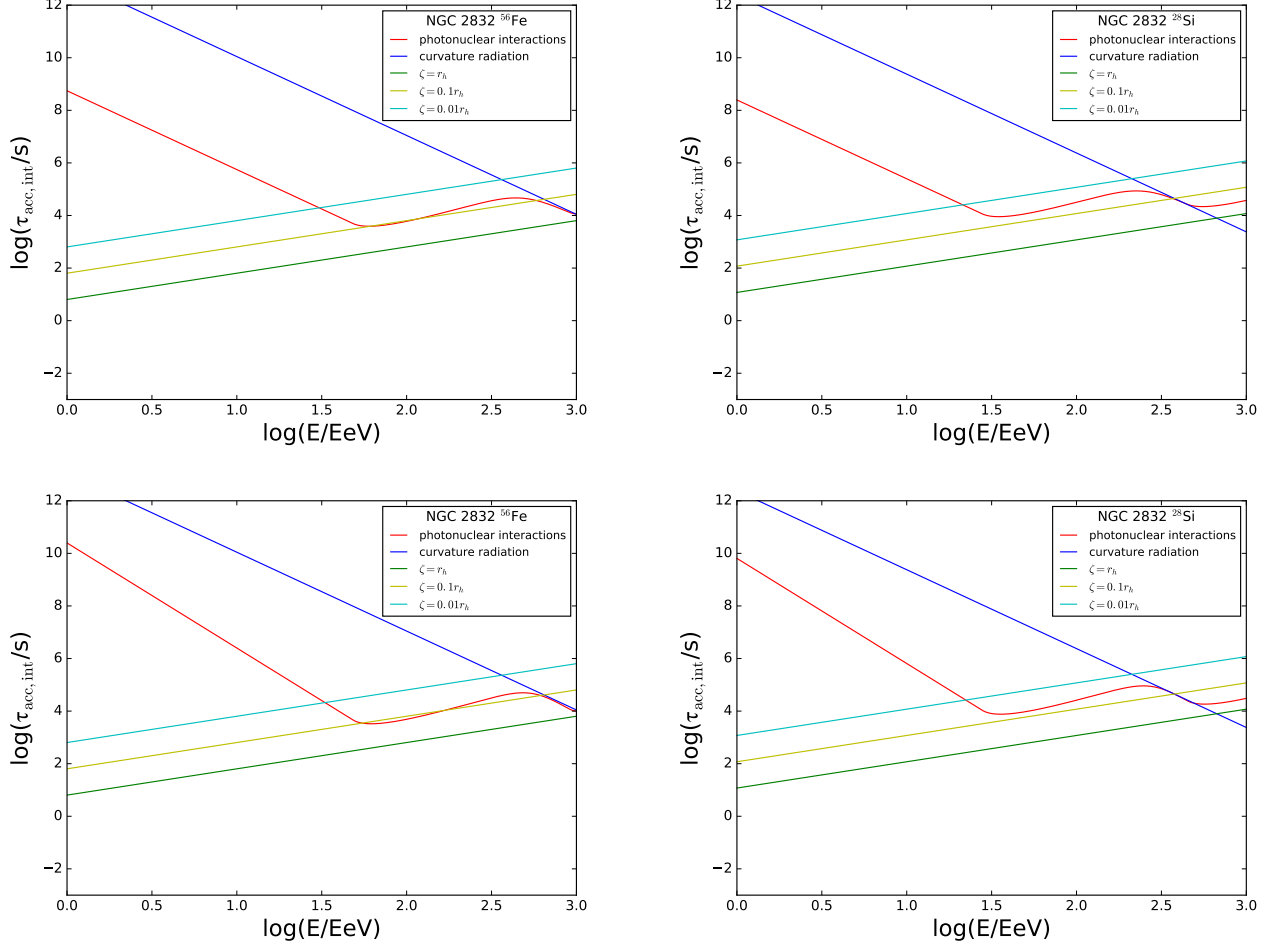
FIG. 4. Comparison of acceleration and interaction time scales for NGC 2832. Conventions are as in Fig. 3.

Note that for our fiducial values $B_4 \sim 1$, $M_9 \sim 1$, and $r_c \sim r_h$, we have $\gamma_{\mathrm{max}}^{\mathrm{acc}} \sim \gamma_{\mathrm{max}}^{\mathrm{rad}}$ if $\zeta \sim r_h$. However, by taking $\zeta < r_h$ one can always suppress the emission of curvature photons. Moreover, as we show in what follows photonuclear interactions on the ambient photon background become the dominant mechanism for energy losses.

The estimation of the photon density in the vicinity of the SMBH is not straightforward. Studies for Cen A are quite extensive [105, 106], and the photon spectrum around the SMBH is consistent with a thermal origin: mostly dust emission heated by the nucleus [105]. For simplicity, in our calculations we approximate the photon spectrum as a broken power-law,

$$n(\varepsilon) = n_0 \begin{cases} (\varepsilon/\varepsilon_0)^{\alpha} & \varepsilon < \varepsilon_0 \\ (\varepsilon/\varepsilon_0)^{\beta} & \text{otherwise}, \end{cases} \quad (23)$$

which is also consistent with the data. Here ε is the photon energy and the maximum of the density is at an energy of ε_0. The broken power-law spectrum allows a complete analytic treatment of photonuclear interactions, and the global result does not depend on the exact shape of the photon spectrum.

Namely, the interaction times are comparable if the photon density is assumed to follow a (modified) black body spectrum [24]. For more distance sources, it is not trivial to disentangle which photons are near the SMBH. As a first approximation, we use the galaxy-wide average far infra-red (FIR) flux reported in the NASA extragalactic database to normalize the spectrum and estimate the spectral indices [107]. If a correlation becomes evident in the future a more detailed analysis would be required. By averaging over the thermal spectra of the sources studied in [108] we take $\alpha = 2$ and $-5 \leq \beta \leq -4$.

We normalize the spectrum to the FIR luminosity in the vicinity of the SMBH

$$L_{\mathrm{FIR}}^{\mathrm{BH}} = 4\pi r_g^2 c \int n(\varepsilon)\, \varepsilon\, d\varepsilon$$
$$= 4\pi r_g^2 c\, n_0 \left\{ \int_{\varepsilon_{\mathrm{min}}}^{\varepsilon_0} (\varepsilon/\varepsilon_0)^{\alpha}\, \varepsilon\, d\varepsilon + \int_{\varepsilon_0}^{\infty} (\varepsilon/\varepsilon_0)^{\beta}\, \varepsilon\, d\varepsilon \right\}, (24)$$

where $\varepsilon_{\mathrm{min}} = 10^{-4}$ eV and $\varepsilon_0 = 10^{-2}$ eV. There is a general consensus that the extended FIR emission along the dust lane of Cen A, $L_{\mathrm{FIR}} \sim 2 \times 10^{10} L_\odot$, cannot only be attributed to dust heated by the active nucleus [109–112]. Optical detections of
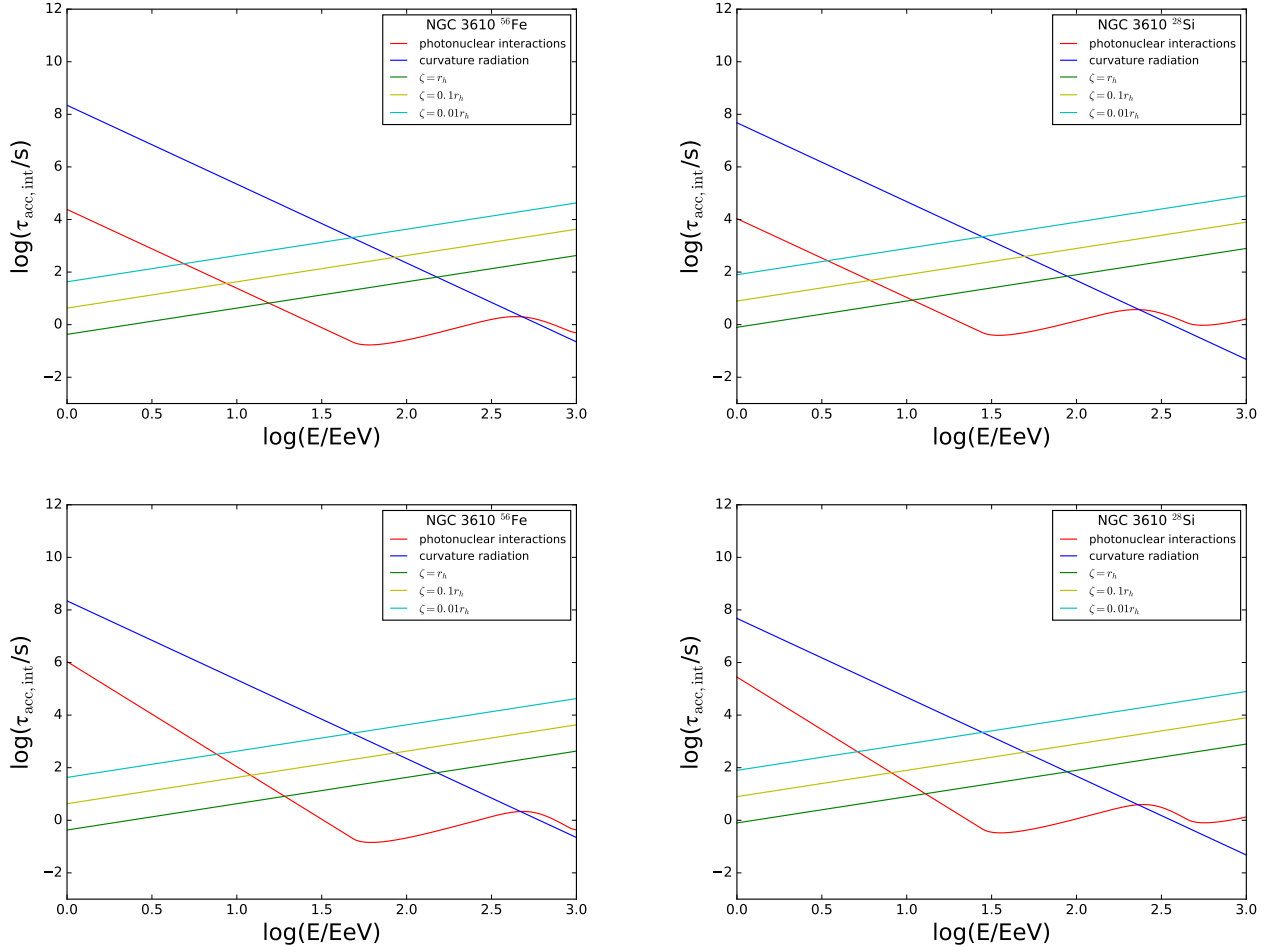
FIG. 5. Comparison of acceleration and interaction time scales for NGC 3610. Conventions are as in Fig. 3.

luminous HII regions in relatively unoscured regions of the dark lane [113] suggest that recently formed stars embedded in the dust lane must be responsible for most of the broadly extended FIR emission. Only about 1% of the FIR emission comes from the active nucleus. With this in mind, we take $L_{\mathrm{FIR}}^{\mathrm{BH}}/L_{\mathrm{FIR}} \sim 10^{-2}$. The normalization factor is then

$$n_0 = \frac{L_{\mathrm{FIR}}^{\mathrm{BH}}}{4\pi\, r_g^2\, c} \left\{ \frac{\varepsilon_0^{-\alpha}}{(\alpha+2)} \left[\varepsilon_0^{\alpha+2} - \varepsilon_{\mathrm{min}}^{\alpha+2} \right] - \frac{\varepsilon_0^2}{(\beta+2)} \right\}^{-1}. \quad (25)$$

In Table I we summarize the relevant properties of a sub-group of 5 candidate sources shown in Fig. 1. In the case of no-detection in the FIR we normalize the photon flux to the reported upper-limit. To determine the distance to these sources we adopt the usual concordance cosmology of a flat universe dominated by a cosmological constant, with $\Omega_\Lambda = 0.692 \pm 0.012$ and a cold dark matter plus baryon component $\Omega_m = 0.308 \pm 0.012$; the Hubble parameter as a function of redshift is given by $H^2(z) = H_0^2[\Omega_m(1+z)^3 + \Omega_\Lambda]$, normalized to its value today, $H_0 = 100\, h\,\mathrm{km\,s^{-1}\,Mpc^{-1}}$, with $h = 0.678$ [118].

To characterize the population of nearby quasar remnants

we also study the case of NGC 5128. This case is special, as the photon spectrum peaks in the mid-infrared. We take $\epsilon_0 = 0.13$ eV and $L_{\mathrm{mid-IR}}/L_\odot = 1.3 \times 10^8$. The mass of the SMBH is somewhat uncertain [119–121]. In our calculations we adopt $M_9 = 0.1$, yielding $n_0^{-4} = 3.0 \times 10^{23}\,\mathrm{MeV^{-1}\,cm^{-3}}$ and $n_0^{-5} = 3.9 \times 10^{23}\,\mathrm{MeV^{-1}\,cm^{-3}}$.

The interaction time for a highly relativistic nucleus propagating through an isotropic photon background with energy ε and spectrum $n(\varepsilon)$, normalized so that the total number of photons in a box is $\int n(\varepsilon)d\varepsilon$, is given by [122]

$$\frac{1}{\tau_{\mathrm{int}}^{A\gamma}} = \frac{c}{2} \int_0^\infty d\varepsilon\, \frac{n(\varepsilon)}{\gamma^2\varepsilon^2} \int_0^{2\gamma\varepsilon} d\varepsilon'\, \varepsilon'\, \sigma(\varepsilon'), \quad (26)$$

where $\sigma(\varepsilon')$ is the photonuclear interaction cross section of a nucleus by a photon energy ε' in the rest frame of the nucleus.

We have found that for the considerations in the present work, the cross section can be safely approximated by the single pole of the narrow-width approximation,

$$\sigma(\varepsilon') = \pi\, \sigma_{\mathrm{res}}\, \frac{\Gamma_{\mathrm{res}}}{2}\, \delta(\varepsilon' - \varepsilon'_{\mathrm{res}}), \quad (27)$$
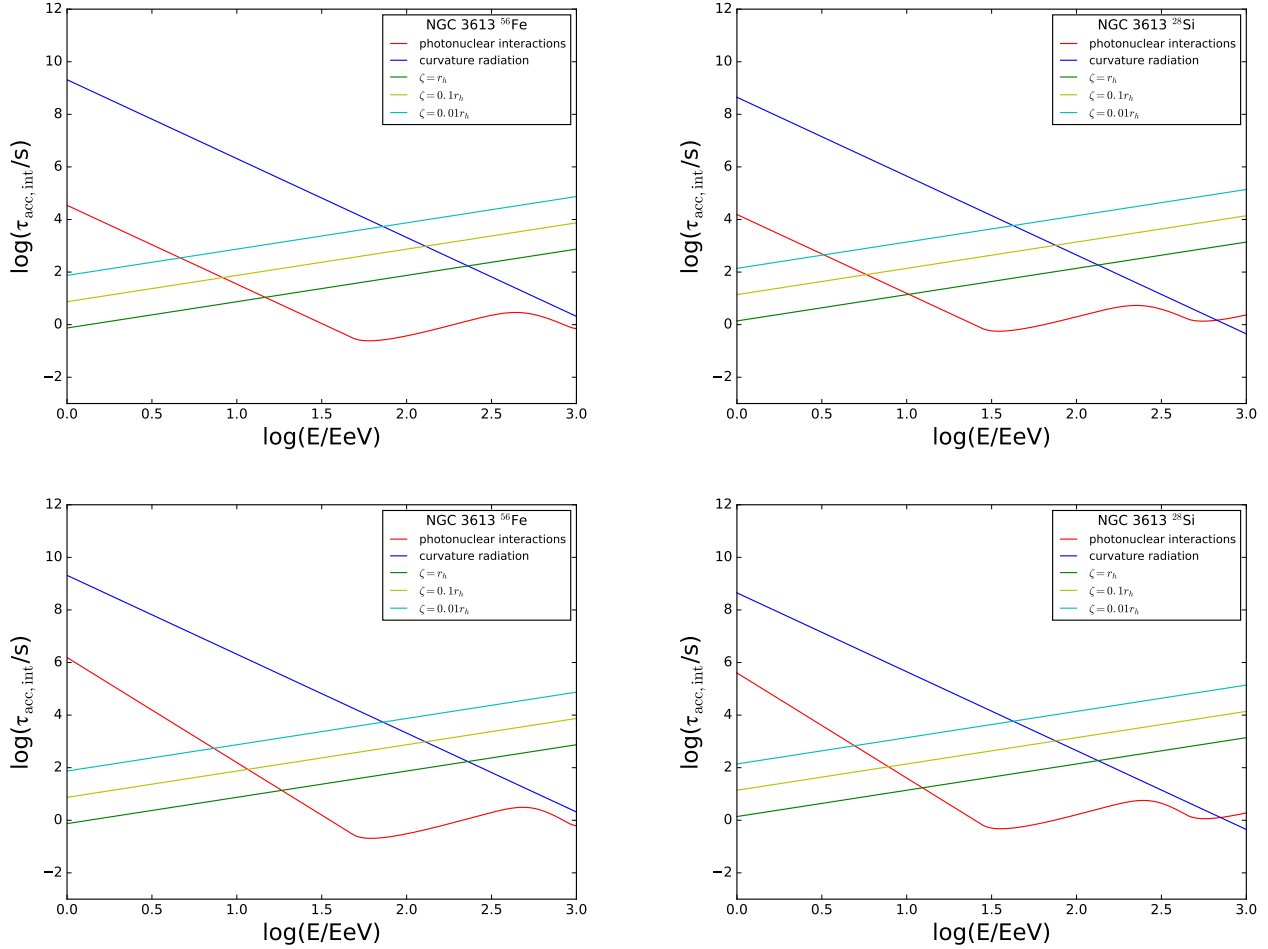
FIG. 6. Comparison of acceleration and interaction time scales for NGC 3613. Conventions are as in Fig. 3.

where σ_{res} is the resonance peak, Γ_{res} its width, and $\varepsilon'_{\text{res}}$ the pole in the rest frame of the nucleus. The factor of $1/2$ is introduced to match the integral (i.e. total cross section) of the Breit-Wigner and the delta function [123].

The mean interaction time can now be readily obtained substituting Eq. (27) into Eq. (26),

$$\frac{1}{\tau_{\text{int}}^{A\gamma}(E)} \approx \frac{c\,\pi\,\sigma_{\text{res}}\,\varepsilon'_{\text{res}}\,\Gamma_{\text{res}}}{4\,\gamma^2} \int_0^\infty \frac{d\varepsilon}{\varepsilon^2}\; n(\varepsilon)\;\Theta(2\gamma\varepsilon - \varepsilon'_{\text{res}})$$
$$= \frac{c\,\pi\,\sigma_{\text{res}}\,\varepsilon'_{\text{res}}\,\Gamma_{\text{res}}}{4\,\gamma^2} \int_{\epsilon'_{\text{res}}/2\gamma}^\infty \frac{d\varepsilon}{\varepsilon^2}\; n(\varepsilon)\,. \qquad (28)$$

Substituting (23) into (28) we finally find [24]

$$\frac{1}{\tau_{\text{int}}^{A\gamma}(E)} = \frac{1}{\tau_b} \begin{cases} (E_b/E)^{\beta+1} & E \le E_b \\ (1-\beta)/(1-\alpha)\left[(E_b/E)^{\alpha+1} - (E_b/E)^2\right] + (E_b/E)^2 & E > E_b \end{cases}, \qquad (29)$$

where

$$\tau_b = \frac{2\,E_b\,(1-\beta)}{c\,\pi\,\sigma_{\text{res}}\,A\,m_p\,\Gamma_{\text{res}}\,n_0} \quad \text{and} \quad E_b = \frac{\varepsilon'_{\text{res}}\,A\,m_p}{2\varepsilon_0}. \qquad (30)$$

The parameters characterizing the photodisintegration cross section are: $\sigma_{\text{res}} \approx 1.45 \times 10^{-27}$ cm^2 A, $\Gamma_{\text{res}} = 8$ MeV, and $\epsilon'_{\text{res}} = 42.65 A^{-0.21}$ $(0.925 A^{2.433})$ MeV, for $A > 4$ $(A \le 4)$ [124].
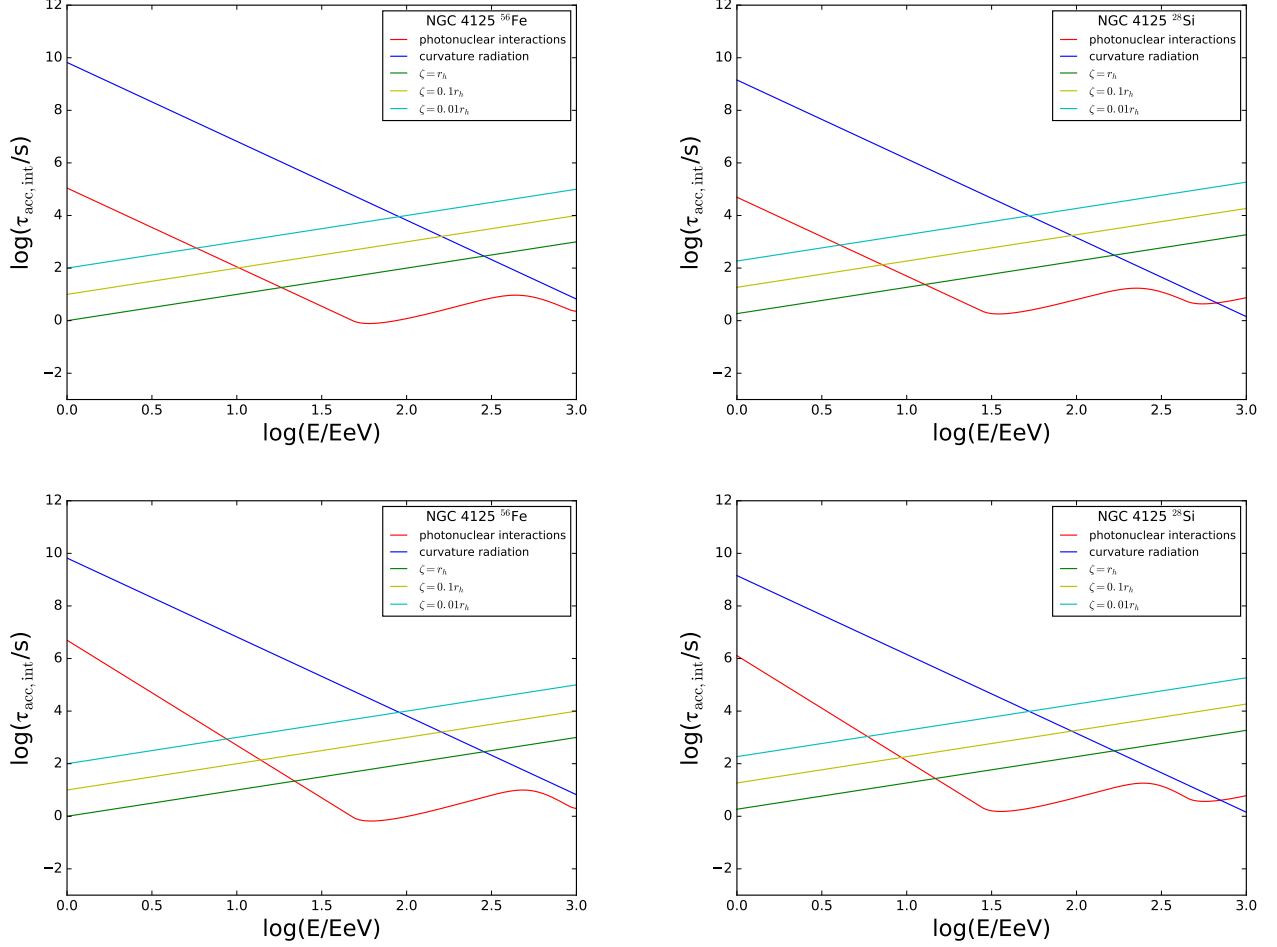
FIG. 7. Comparison of acceleration and interaction time scales for NGC 4125. Conventions are as in Fig. 3.

The parameters for the photopion production cross section are: $\sigma_{\rm res} \simeq 5.0 \times 10^{-28}$ cm$^2\, A$, $\Gamma_{\rm res} = 150$ MeV, and $\varepsilon'_{\rm res} = (m_\Delta^2 - m_p^2)/(2m_p) \simeq 340$ MeV [118].

In Figs. 3, 4, 5, 6, 7, and 8 we compare the characteristic time scales of acceleration and energy losses for the various representative sources given in Table I and Cen A. We consider ^{56}Fe and ^{28}Si as fiducial nuclear species. In general, photonuclear interactions dominate the energy losses. By comparing the results for $\beta = -5$ and $\beta = -4$, we can see that there is almost no dependence on the photon spectral index. For $E \gtrsim 10^{11}$ GeV, the accelerated nuclei reach the photopion production threshold, and the significance of this process becomes more important with increasing energy. The photopion production threshold corresponds to an energy-per-nucleon of $E/A \sim 10^{10}$ GeV. Note that the onset of photopion production is above the required maximum energy $= 10^{9.5}$ GeV for the fiducial model in [24]. Therefore, we conclude that some quasar remnants are capable of launching heavy (and medium mass) nuclei up to the observed maximum energies.

Though Figs. 3, 4, 5, 6, 7, and 8 provide only a naïve illustration of particle acceleration with energy dissipation in the black hole dynamo it is evident that it possible to classify the one-shot acceleration mechanism in quasar remnants according to how source parameters (mass of the central engine and the ambient photon backgrounds) impact the photonuclear interaction. In the first type nuclei are completely photodisintegrated before escaping the acceleration region producing a flux of secondary nucleons, e.g. NGC 2768, 3610, 3613, 4125, and 5128. In the second type photopion production is the major energy damping mechanism and nuclei are able to escape without suffering significant spallation, e.g. NGC 2832 (which is near the center of the TA hot-spot). Combining the ideas put forward in [23, 24] we can now formulate a new hybrid model to explain the spectral shape of extragalactic cosmic rays, including the critical region of the ankle. Namely, the secondary nucleons produced in the photodisintegration process would have a soft spectral index at the source, and consequently can explain the energy region below the ankle. Note that after the photodisintegration process the secondary protons can still be accelerated to reach energies near the ankle. On the other hand, heavy and medium mass nuclei are emitted with a harder spectral index, and therefore (upon propagation to Earth) can populate the spectrum above the ankle, all the way to the GZK cutoff. We estimate that about 16%
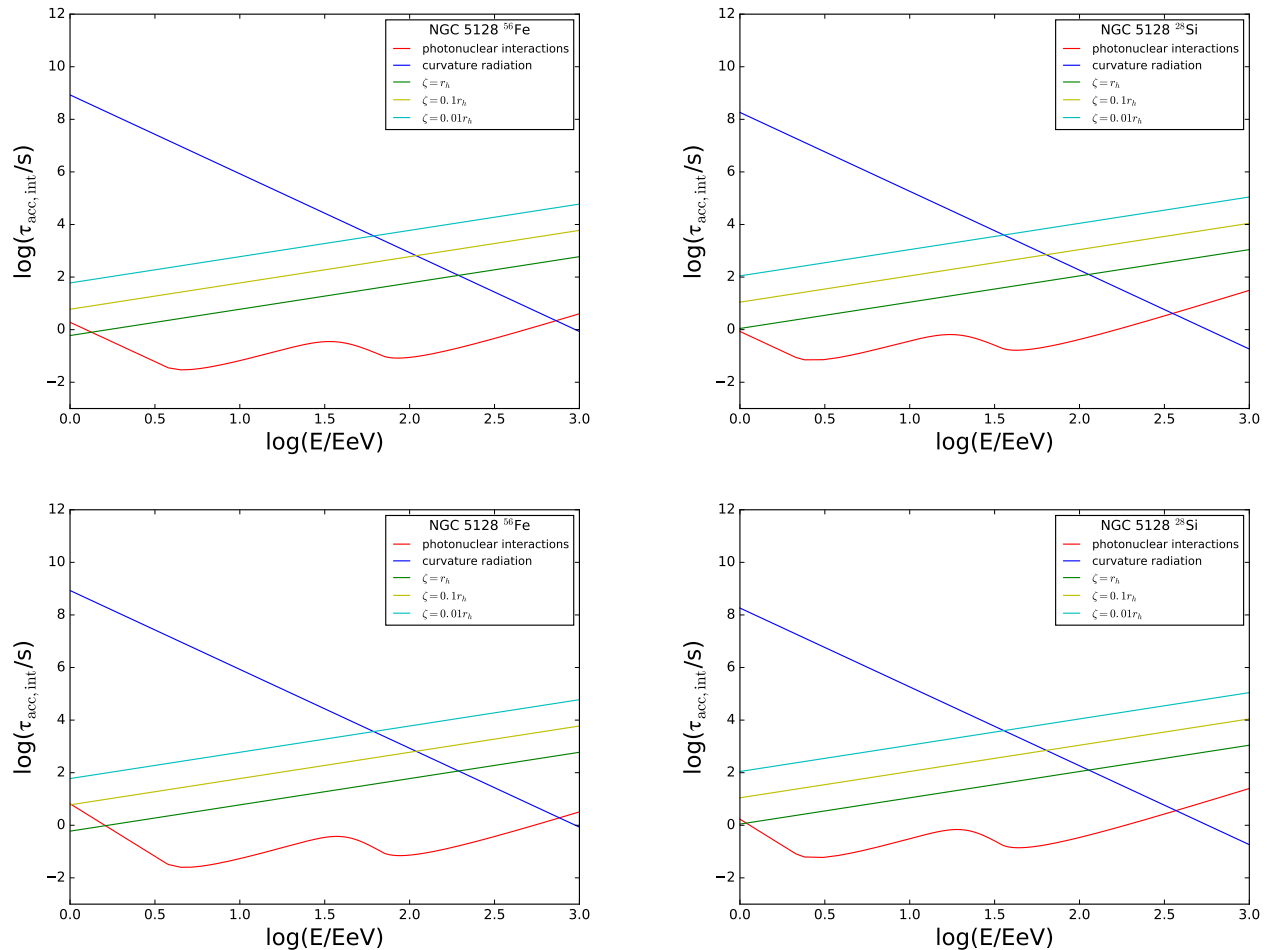
FIG. 8. Comparison of acceleration and interaction time scales for NGC 5128. Conventions are as in Fig. 3.

of the SMBH in the universe could accelerate UHECR nuclei via the BZ. At this stage, it is worthwhile to point out that for SMBHs associated with jets terminating in lobes (which can be detected in radio) like Cen A other cosmic ray acceleration mechanisms may be at play [125–127].

It is also possible that the emitted nuclei could suffer additional photodisintegration while diffusing in the source environment, as described in [24]. Photodisintegration of high-energy nuclei, $A + \gamma \rightarrow A'^* + X$, is followed by immediate photoemission from the excited daughter nuclei, $A'^* \rightarrow A' + \gamma$ [128]. The photodisintegration process in the source environment would then produce a flux of gamma-rays. A suggestion of a correlation between UHECRs and nearby gamma-ray emitting AGNs has been put forward in [129]. Such a correlation would be consistent with our model. However, we should exercise caution since the results in [129] are given with an *a posteriori* significance, and since the new AGN correlation analyses has not shown an increased in significance over time [83].

In closing, we study the dependence of our conclusions on the magnetic field strength. As we have shown, the SMBHs which are capable of emitting UHECR nuclei without suffer-ing significant spallation are those with masses $\gtrsim 10^{10} M_\odot$. We can then rewrite the acceleration time scale (17) keeping B_4 as a variable, i.e. we take

$$\tau_{\rm acc} = \frac{E}{10^{11} \text{ GeV}} \frac{1}{ZM_9 B_4} \frac{r_h^2}{\zeta c}. \tag{31}$$

In Fig. 9 we compare the acceleration and interaction time scales for different magnetic field strengths. As we anticipated in Sec. II, by simple inspection of Fig. 9 one can see that CR nuclei can be accelerated to the highest observed energies with $B_4 \gtrsim 0.01$.

V. CONCLUSIONS

We have investigated the possibility of UHECRs being accelerated in nearby supermassive black holes, which are dormant remnants of previously active quasars. We have shown that these fast spinning objects are latent dynamos that can accelerate heavy nuclei up to the maximum observed energies. We have also shown that energy losses are dominated by photonuclear interactions on the ambient photon fields. Armed
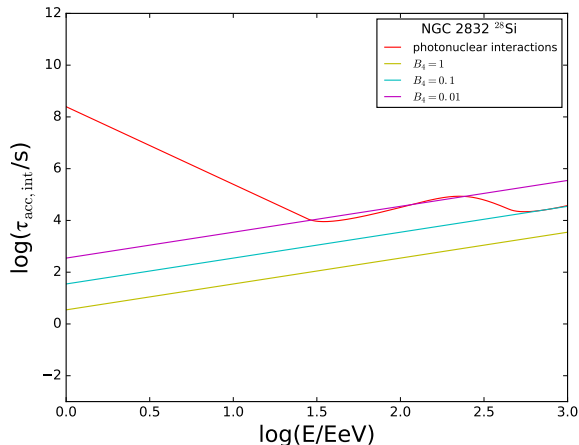
fore escaping the acceleration region producing a flux of secondary nucleons. In the second type photopion production is the major energy damping mechanism and nuclei are able to escape without suffering significant spallation. In the spirit of [23, 24] we conjectured that the spectral shape of extragalactic cosmic rays, including the pivotal region of the ankle, can be described by a smooth superposition of these two type of sources. Namely, the secondary nucleons produced in the photodisintegration process would have a soft spectral index at the source, and consequently can explain the energy region below the ankle. On the other hand, heavy and medium mass nuclei are emitted with a harder spectral index, and therefore (upon propagation to Earth) can populate the spectrum above the ankle, all the way to the GZK cutoff.

FIG. 9. Comparison of acceleration and interaction time scales for NGC 2832. The bumpy curve indicates the interaction time scale for photonuclear interactions. The straight lines (with positive slope) correspond to acceleration time scales with different magnetic field strengths; namely, $B_4 = 1, 0.1, 0.01$. We have taken $\zeta = 0.01 r_h$ and $\beta = -4$.

with our findings we postulated a classification scheme for giant elliptical galaxies harboring supermassive black hole dynamos. In this classification we distinguish among two unequivocal type of cosmic ray sources according on how source parameters (mass of the central engine and the ambient photon backgrounds) impact the photonuclear interaction. In the first type nuclei are completely photodisintegrated be-

[1] D. F. Torres and L. A. Anchordoqui, Astrophysical origins of ultrahigh energy cosmic rays, Rept. Prog. Phys. **67**, 1663 (2004) doi:10.1088/0034-4885/67/9/R03 [astro-ph/0402371].

[2] K. Kotera and A. V. Olinto, The astrophysics of ultrahigh energy cosmic rays, Ann. Rev. Astron. Astrophys. **49**, 119 (2011) doi:10.1146/annurev-astro-081710-102620 [arXiv:1101.4256 [astro-ph.HE]].

[3] R. U. Abbasi *et al.* [HiRes Collaboration], First observation of the Greisen-Zatsepin-Kuzmin suppression, Phys. Rev. Lett. **100**, 101101 (2008) doi:10.1103/PhysRevLett.100.101101 [astro-ph/0703099].

[4] J. Abraham *et al.* [Pierre Auger Collaboration], Observation of the suppression of the flux of cosmic rays above 4×10^{19} eV, Phys. Rev. Lett. **101**, 061101 (2008) doi:10.1103/PhysRevLett.101.061101 [arXiv:0806.4302 [astro-ph]].

[5] J. Abraham *et al.* [Pierre Auger Collaboration], Measurement of the energy spectrum of cosmic rays above 10^{18} eV using the Pierre Auger Observatory, Phys. Lett. B **685**, 239 (2010) doi:10.1016/j.physletb.2010.02.013 [arXiv:1002.1975 [astro-ph.HE]].

[6] D. J. Bird *et al.* [HiRes Collaboration], Evidence for correlated changes in the spectrum and composition of cosmic rays at extremely high-energies, Phys. Rev. Lett. **71**, 3401 (1993) doi:10.1103/PhysRevLett.71.3401.

[7] D. Allard, E. Parizot, E. Khan, S. Goriely and A. V. Olinto, UHE nuclei propagation and the interpretation of the ankle in the cosmic-ray spectrum, Astron. Astrophys. **443**, L29 (2005) doi:10.1051/0004-6361:200500199 [astro-ph/0505566].

[8] D. Allard, E. Parizot and A. V. Olinto, On the transition from galactic to extragalactic cosmic-rays: spectral and composition features from two opposite scenarios, Astropart. Phys. **27**, 61 (2007) doi:10.1016/j.astropartphys.2006.09.006 [astro-ph/0512345].

[9] K. Greisen, End to the cosmic ray spectrum?, Phys. Rev. Lett. **16**, 748 (1966) doi:10.1103/PhysRevLett.16.748.

[10] G. T. Zatsepin and V. A. Kuzmin, Upper limit of the spectrum of cosmic rays, JETP Lett. **4**, 78 (1966) [Pisma Zh. Eksp. Teor. Fiz. **4**, 114 (1966)].

[11] M. Hillas, The energy spectrum of cosmic rays in an evolving universe, Phys. Lett. A **24**, 677 (1967) doi:10.1016/0375-9601(67)91023-7.

[12] V. Berezinsky, A. Z. Gazizov and S. I. Grigorieva, On astrophysical solution to ultrahigh-energy cosmic rays, Phys. Rev. D **74**, 043005 (2006) doi:10.1103/PhysRevD.74.043005 [hep-ph/0204357].

[13] K. H. Kampert and M. Unger, Measurements of the cosmic ray composition with air shower experiments, Astropart. Phys. **35**, 660 (2012) doi:10.1016/j.astropartphys.2012.02.004 [arXiv:1201.0018 [astro-ph.HE]].

[14] A. Aab *et al.* [Pierre Auger Collaboration], Depth of maximum of air-shower profiles at the Pierre Auger Observatory I: Measurements at energies above $10^{17.8}$ eV, Phys. Rev. D **90**, no. 12, 122005 (2014) doi:10.1103/PhysRevD.90.122005 [arXiv:1409.4809 [astro-ph.HE]].

[15] A. Aab *et al.* [Pierre Auger Collaboration], Depth of maximum of air-shower profiles at the Pierre Auger Observatory II: Composition implications, Phys. Rev. D **90**, no. 12, 122006 (2014) doi:10.1103/PhysRevD.90.122006 [arXiv:1409.5083 [astro-ph.HE]].

[16] A. Aab *et al.* [Pierre Auger Collaboration], Evidence for a mixed mass composition at the ankle in the cosmic-ray spectrum, Phys. Lett. B **762**, 288 (2016) doi:10.1016/j.physletb.2016.09.039 [arXiv:1609.08567 [astro-ph.HE]].

[17] A. Aab *et al.* [Pierre Auger Collaboration], Combined fit of spectrum and composition data as measured by the Pierre Auger Observatory, [arXiv:1612.07155 [astro-ph.HE]].

[18] P. Abreu *et al.* [Pierre Auger Collaboration], Large scale distribution of arrival directions of cosmic rays detected above 10^{18} eV at the Pierre Auger Observatory, Astrophys. J. Suppl. **203**, 34 (2012) doi:10.1088/0067-0049/203/2/34 [arXiv:1210.3736 [astro-ph.HE]].

[19] A. Aab *et al.* [Pierre Auger Collaboration], Large scale distribution of ultrahigh energy cosmic rays detected at the Pierre Auger Observatory with zenith angles up to $80°$, Astrophys. J. **802**, no. 2, 111 (2015) doi:10.1088/0004-637X/802/2/111 [arXiv:1411.6953 [astro-ph.HE]].

[20] R. U. Abbasi *et al.*, Study of ultrahigh energy cosmic ray composition using Telescope Arrays Middle Drum detector and surface array in hybrid mode, Astropart. Phys. **64**, 49 (2014) doi:10.1016/j.astropartphys.2014.11.004 [arXiv:1408.1726 [astro-ph.HE]].

[21] R. Abbasi *et al.* [Pierre Auger and Telescope Array Collaborations], Report of the working group on the composition of ultrahigh energy cosmic rays, arXiv:1503.07540 [astro-ph.HE].

[22] R. U. Abbasi *et al.* [Telescope Array Collaboration], Indications of intermediate-scale anisotropy of cosmic rays with energy greater than 57 EeV in the Northern sky measured with the surface detector of the Telescope Array experiment, Astrophys. J. **790**, L21 (2014) doi:10.1088/2041-8205/790/2/L21 [arXiv:1404.5890 [astro-ph.HE]].

[23] R. Aloisio, V. Berezinsky and P. Blasi, Ultrahigh energy cosmic rays: implications of Auger data for source spectra and chemical composition, JCAP **1410**, no. 10, 020 (2014) doi:10.1088/1475-7516/2014/10/020 [arXiv:1312.7459 [astro-ph.HE]].

[24] M. Unger, G. R. Farrar and L. A. Anchordoqui, Origin of the ankle in the ultrahigh energy cosmic ray spectrum, and of the extragalactic protons below it, Phys. Rev. D **92**, no. 12, 123001 (2015) doi:10.1103/PhysRevD.92.123001 [arXiv:1505.02153 [astro-ph.HE]].

[25] G. R. Farrar, M. Unger and L. A. Anchordoqui, Origin of the ankle in the ultra-high energy cosmic ray spectrum and the extragalactic protons below it, arXiv:1512.00484 [astro-ph.HE].

[26] N. Globus, D. Allard and E. Parizot, A complete model of the cosmic ray spectrum and composition across the Galactic to extragalactic transition, Phys. Rev. D **92**, no. 2, 021302 (2015) doi:10.1103/PhysRevD.92.021302 [arXiv:1505.01377 [astro-ph.HE]].

[27] L. A. Anchordoqui, Neutron β-decay as the origin of IceCubes PeV (anti)neutrinos, Phys. Rev. D **91**, 027301 (2015) doi:10.1103/PhysRevD.91.027301 [arXiv:1411.6457 [astro-ph.HE]].

[28] A. M. Taylor, M. Ahlers and D. Hooper, Indications of negative evolution for the sources of the highest energy cosmic rays, Phys. Rev. D **92**, no. 6, 063011 (2015) doi:10.1103/PhysRevD.92.063011 [arXiv:1505.06090 [astro-ph.HE]].

[29] M. Ackermann *et al.* [Fermi-LAT Collaboration], The spectrum of isotropic diffuse gamma-ray emission between 100 MeV and 820 GeV, Astrophys. J. **799**, 86 (2015) doi:10.1088/0004-637X/799/1/86 [arXiv:1410.3696 [astro-ph.HE]].

[30] M. Ackermann *et al.* [Fermi-LAT Collaboration], Resolving the extragalactic γ-ray background above 50 GeV with the Fermi Large Area Telescope, Phys. Rev. Lett. **116**, no. 15, 151105 (2016) doi:10.1103/PhysRevLett.116.151105 [arXiv:1511.00693 [astro-ph.CO]].

[31] R. Y. Liu, A. M. Taylor, X. Y. Wang and F. A. Aharonian, Indication of a local fog of subankle ultrahigh energy cosmic rays, Phys. Rev. D **94**, no. 4, 043008 (2016) doi:10.1103/PhysRevD.94.043008 [arXiv:1603.03223 [astro-ph.HE]].

[32] E. Boldt and P. Ghosh, Cosmic rays from remnants of quasars?, Mon. Not. Roy. Astron. Soc. **307**, 491 (1999) doi:10.1046/j.1365-8711.1999.02600.x [astro-ph/9902342].

[33] E. Boldt and M. Loewenstein, Cosmic ray generation by quasar remnants: Constraints and implications, Mon. Not. Roy. Astron. Soc. **316**, L29 (2000) doi:10.1046/j.1365-8711.2000.03768.x [astro-ph/0006221].

[34] D. F. Torres, E. Boldt, T. Hamilton and M. Loewenstein, Nearby quasar remnants and ultrahigh-energy cosmic rays, Phys. Rev. D **66**, 023001 (2002) doi:10.1103/PhysRevD.66.023001 [astro-ph/0204419].

[35] A. Y. Neronov, D. V. Semikoz and I. I. Tkachev, Ultra-high energy cosmic ray production in the polar cap regions of black hole magnetospheres, New J. Phys. **11**, 065015 (2009) doi:10.1088/1367-2630/11/6/065015 [arXiv:0712.1737 [astro-ph]].

[36] R. D. Blandford and R. L. Znajek, Electromagnetic extractions of energy from Kerr black holes, Mon. Not. Roy. Astron. Soc. **179**, 433 (1977).

[37] R. L. Znajek The electric and magnetic conductivity of a Kerr hole, Mon. Not. Roy. Astron. Soc. **185**, 833 (1978).

[38] C. Hazard, M. B. Mackey and A. J. Shimmins, Investigation of the radio source 3C 273 by the method of lunar occultations, Nature **197**, 1037 (1963). doi:10.1038/1971037a0

[39] M. Schmidt 3C 273 : A star-like object with large red-shift, Nature **197**, 1040 (1963). doi:10.1038/1971040a0

[40] H. J. Smith and D. Hoffleit Light variations in the superluminous radio galaxy 3C273, Nature **198**, 650 (1963). doi:10.1038/198650a0

[41] Ya B. Zeldovich and I. D. Novikov, Mass of quasi-stellar objects, Doklady Acad. Nauk SSSR **158**, 811 [Sov. Phys.-Doklady **9**, 834 (1965)].

[42] E. E. Salpeter, Accretion of interstellar matter by massive objects, Astrophys. J. **140**, 796 (1964). doi:10.1086/147973

[43] D. Lynden-Bell, Galactic nuclei as collapsed old quasars, Nature **223**, 690 (1969). doi:10.1038/223690a0

[44] R. Antonucci, Unified models for active galactic nuclei and quasars, Ann. Rev. Astron. Astrophys. **31**, 473 (1993). doi:10.1146/annurev.aa.31.090193.002353

[45] C. M. Urry and P. Padovani, Unified schemes for radio-loud active galactic nuclei, Publ. Astron. Soc. Pac. **107**, 803 (1995) doi:10.1086/133630 [astro-ph/9506063].

[46] A. S. Eddington, A limiting case in the theory of radiative equilibrium, Mon. Not. Roy. Astron. Soc. **85**, 408 (1925) doi:10.1093/mnras/85.5.408

[47] N. I. Shakura and R. A. Sunyaev, Black holes in binary systems: Observational appearance, Astron. Astrophys. **24**, 337 (1973).

[48] M. J. Rees, "Dead quasars" in nearby galaxies, Science **247**, 817 (1990) doi: 10.1126/science.247.4944.817

[49] D. Richstone *et al.*, Supermassive black holes and the evolution of galaxies, Nature **395**, A14 (1998) [astro-ph/9810378].

[50] L. C. Ho, What powers the compact radio emission in nearby elliptical and SO galaxies?, Astrophys. J. **510**, 631 (1999) doi:10.1086/306597 [astro-ph/9808123].

[51] J. Kormendy and R. Kennicutt, Jr., Secular evolution and the formation of pseudobulges in disk galaxies, Ann. Rev. Astron. Astrophys. **42**, 603 (2004) doi:10.1146/annurev.astro.42.053102.134024 [astro-ph/0407343].

[52] J. Kormendy and D. Richstone, Inward bound: The search for supermassive black holes in galactic nuclei, Ann. Rev. Astron. Astrophys. **33** (1995) 581. doi:10.1146/annurev.aa.33.090195.003053

[53] J. Magorrian *et al.*, The demography of massive dark objects in galaxy centers, Astron. J. **115**, 2285 (1998) doi:10.1086/300353 [astro-ph/9708072].

[54] K. Gebhardt *et al.*, A relationship between nuclear black hole mass and galaxy velocity dispersion, Astrophys. J. **539**, L13 (2000) doi:10.1086/312840 [astro-ph/0006289].

[55] L. Ferrarese and D. Merritt, A fundamental relation between supermassive black holes and their host galaxies, Astrophys. J. **539**, L9 (2000) doi:10.1086/312838 [astro-ph/0006053].

[56] N. Haring and H. W. Rix, On the black hole mass-bulge mass relation, Astrophys. J. **604**, L89 (2004) doi:10.1086/383567 [astro-ph/0402376].

[57] M. Vika, S. P. Driver, A. W. Graham and J. Liske, The millennium galaxy catalogue: The $M_{BH} - L_{spheroid}$ derived supermassive black hole mass function, Mon. Not. Roy. Astron. Soc. **400**, 1451 (2009) doi:10.1111/j.1365-2966.2009.15544.x [arXiv:0908.2102 [astro-ph.CO]].

[58] R. J. McLure and J. S. Dunlop, The cosmological evolution of quasar black-hole masses, Mon. Not. Roy. Astron. Soc. **352**, 1390 (2004) doi:10.1111/j.1365-2966.2004.08034.x [astro-ph/0310267].

[59] A. W. Graham, S. P. Driver, P. D. Allen and J. Liske, The millennium galaxy catalogue: The local supermassive black hole mass function in early- and late-type galaxies, Mon. Not. Roy. Astron. Soc. **378**, 198 (2007) doi:10.1111/j.1365-2966.2007.11770.x [arXiv:0704.0316 [astro-ph]].

[60] A. Marconi, G. Risaliti, R. Gilli, L. K. Hunt, R. Maiolino and M. Salvati, Local supermassive black holes, relics of active galactic nuclei and the X-ray background, Mon. Not. Roy. Astron. Soc. **351**, 169 (2004) doi:10.1111/j.1365-2966.2004.07765.x [astro-ph/0311619].

[61] N. Tamura, K. Ohta and Y. Ueda, Supermassive black hole mass functions at intermediate redshifts from spheroid and AGN luminosity functions, Mon. Not. Roy. Astron. Soc. **365**, 134 (2006) doi:10.1111/j.1365-2966.2005.09677.x [astro-ph/0509912].

[62] A. Soltan, Masses of quasars, Mon. Not. Roy. Astron. Soc. **200**, 115 (1982).

[63] A. Chokshi and E. L. Turner Remnants of the quasars, Mon. Not. Roy. Astron. Soc. **259**, 421 (1992). doi: 10.1093/mnras/259.3.421

[64] T. A. Small and R. D. Blandford, Quasar evolution and the growth of black holes, Mon. Not. Roy. Astron. Soc. 259, 725 (1992).

[65] X. Cao and F. Li, Rapidly spinning massive black holes in active galactic nuclei: evidence from the black hole mass function, Mon. Not. Roy. Astron. Soc. **390**, 561 (2008) doi:10.1111/j.1365-2966.2008.13800.x [arXiv:0808.0759 [astro-ph]].

[66] Y. R. Li, L. C. Ho and J. M. Wang, Cosmological evolution of supermassive black holes I: mass function at 0, Astrophys. J. **742**, 33 (2011) doi:10.1088/0004-637X/742/1/33 [arXiv:1109.0089 [astro-ph.CO]].

[67] F. Shankar, D. H. Weinberg and J. Miralda-Escude, Self-consistent models of the AGN and black hole populations: Duty cycles, accretion rates, and the mean radiative efficiency, Astrophys. J. **690**, 20 (2009) doi:10.1088/0004-637X/690/1/20 [arXiv:0710.4488 [astro-ph]].

[68] Q. j. Yu and S. Tremaine, Observational constraints on growth of massive black holes, Mon. Not. Roy. Astron. Soc. **335**, 965 (2002) doi:10.1046/j.1365-8711.2002.05532.x [astro-ph/0203082].

[69] M. Volonteri, M. Sikora and J. P. Lasota, Black-hole spin and galactic morphology, Astrophys. J. **667**, 704 (2007) doi:10.1086/521186 [arXiv:0706.3900 [astro-ph]].

[70] L. A. Anchordoqui, Neutrino lighthouse powered by Sagittarius A* disk dynamo, Phys. Rev. D **94**, 023010 (2016) doi:10.1103/PhysRevD.94.023010 [arXiv:1606.01816 [astro-ph.HE]].

[71] R. D. Blandford and M. J. Rees, Extended and compact extragalactic interpretation and theory Phys. Scripta **17**, 265 (1978).

[72] M. J. M. Marcha, I. W. A. Browne, C. D. Impey and P. S. Smith, Optical spectroscopy and polarization of a new sample of optically bright flat radio spectrum sources Mon. Not. Roy. Astron. Soc. **281**, 425 (1996) doi:10.1093/mnras/281.2.425.

[73] P. Giommi, P. Padovani, G. Polenta, S. Turriziani, V. D'Elia and S. Piranomonte, A simplified view of blazars: clearing the fog around long-standing selection effects, Mon. Not. Roy. Astron. Soc. **420**, 2899 (2012) doi:10.1111/j.1365-2966.2011.20044.x [arXiv:1110.4706 [astro-ph.CO]].

[74] A. Cavaliere and V. D'Elia, The blazar main sequence, Astrophys. J. **571**, 226 (2002) doi:10.1086/339778 [astro-ph/0106512].

[75] M. Boettcher and C. D. Dermer, An evolutionary scenario for blazar unification, Astrophys. J. **564**, 86 (2002) doi:10.1086/324134 [astro-ph/0106395].

[76] M. Ajello *et al.*, The luminosity function of Fermi-detected flat-spectrum radio quasars, Astrophys. J. **751**, 108 (2012) doi:10.1088/0004-637X/751/2/108 [arXiv:1110.3787 [astro-ph.CO]].

[77] M. Ajello *et al.*, The cosmic evolution of Fermi BL Lacertae objects, Astrophys. J. **780**, 73 (2014) doi:10.1088/0004-637X/780/1/73 [arXiv:1310.0006 [astro-ph.CO]].

[78] L. Maraschi and F. Tavecchio, The jet-disk connection and blazar unification, Astrophys. J. **593**, 667 (2003) doi:10.1086/342118 [astro-ph/0205252].

[79] C. Lintott *et al.*, Galaxy zoo : "Hanny's Voorwerp", a quasar light echo?, Mon. Not. Roy. Astron. Soc. **399**, 129 (2009) doi:10.1111/j.1365-2966.2009.15299.x [arXiv:0906.5304 [astro-ph.CO]].

[80] G. I. G. Jozsa *et al.*, Revealing Hanny's Voorwerp: radio observations of IC 2497, Astron. Astrophys. **500**, L33 (2009) doi:10.1051/0004-6361/200912402 [arXiv:0905.1851 [astro-ph.CO]].

[81] H. Rampadarath *et al.*, Hanny's Voorwerp: Evidence of AGN activity and a nuclear starburst in the central regions of IC 2497, Astron. Astrophys. **517**, L8 (2010) doi:10.1051/0004-6361/201014782 [arXiv:1006.4096 [astro-ph.GA]].

[82] K. Schawinski *et al.*, The sudden death of the nearest quasar, Astrophys. J. **724**, L30 (2010) doi:10.1088/2041-8205/724/1/L30 [arXiv:1011.0427 [astro-ph.CO]].

[83] A. Aab *et al.* [Pierre Auger Collaboration], Searches for anisotropies in the arrival directions of the highest energy cosmic rays detected by the Pierre Auger Observatory, Astrophys. J. **804**, no. 1, 15 (2015) doi:10.1088/0004-637X/804/1/15 [arXiv:1411.6111 [astro-ph.HE]].

[84] P. Abreu *et al.* [Pierre Auger Collaboration], Update on the correlation of the highest energy cosmic rays with nearby extragalactic matter, Astropart. Phys. **34**, 314 (2010) doi:10.1016/j.astropartphys.2010.08.010 [arXiv:1009.1855 [astro-ph.HE]].

[85] J. Abraham *et al.* [Pierre Auger Collaboration], Correlation of the highest-energy cosmic rays with the positions of nearby active galactic nuclei, Astropart. Phys. **29**, 188 (2008) Erratum: [Astropart. Phys. **30**, 45 (2008)] doi:10.1016/j.astropartphys.2008.06.004, 10.1016/j.astropartphys.2008.01.002 [arXiv:0712.2843 [astro-ph]].

[86] J. Abraham *et al.* [Pierre Auger Collaboration], Correlation of the highest energy cosmic rays with nearby extragalactic objects, Science **318**, 938 (2007) doi:10.1126/science.1151124 [arXiv:0711.2256 [astro-ph]].

[87] C. Isola, G. Sigl and G. Bertone, Ultrahigh energy cosmic rays from quasar remnants, astro-ph/0312374.

[88] G. Cavallo, On the sources of ultra-high energy cosmic rays, Astron. Astrophys. **65**, 415 (1978).

[89] G. E. Romero, J. A. Combi, L. A. Anchordoqui and S. E. Perez Bergliaffa, A possible source of extragalactic cosmic rays with arrival energies beyond the GZK cutoff, Astropart. Phys. **5**, 279 (1996) doi:10.1016/0927-6505(96)00029-1 [gr-qc/9511031].

[90] B. R. Dawson *et al.* [Pierre Auger and Yakutsk and Telescope Array Collaborations], The energy spectrum of cosmic rays at the highest energies, EPJ Web Conf. **53**, 01005 (2013) doi:10.1051/epjconf/20135301005 [arXiv:1306.6138 [astro-ph.HE]].

[91] J. H. Adams *et al.*, White paper on EUSO-SPB2, arXiv:1703.04513 [astro-ph.HE].

[92] R. P. Kerr, Gravitational field of a spinning mass as an example of algebraically special metrics, Phys. Rev. Lett. **11**, 237 (1963). doi:10.1103/PhysRevLett.11.237

[93] K. Schwarzschild, On the gravitational field of a mass point according to Einstein's theory, Sitzungsber. Preuss. Akad. Wiss. Berlin (Math. Phys.) **1916**, 189 (1916) [physics/9905030].

[94] K. S. Thorne, Disk accretion onto a black hole 2: Evolution of the hole, Astrophys. J. **191**, 507 (1974). doi:10.1086/152991

[95] M. Visser, The Kerr spacetime: A Brief introduction, arXiv:0706.0622 [gr-qc].

[96] F. M. Rieger, Non-thermal processes in black-hole-jet magnetospheres, Int. J. Mod. Phys. D **20**, 1547 (2011) doi:10.1142/S0218271811019712 [arXiv:1107.2119 [astro-ph.CO]].

[97] R. Penrose, Gravitational collapse: The role of general relativity, Riv. Nuovo Cim. **1**, 252 (1969) [Gen. Rel. Grav. **34**, 1141 (2002)].

[98] R. Penrose and R. M. Floyd, Extraction of rotational energy from a black hole, Nature **229**, 177 (1971).

[99] R. M. Wald, Black hole in a uniform magnetic field, Phys. Rev. D **10**, 1680 (1974). doi:10.1103/PhysRevD.10.1680

[100] P. Blasi, R. I. Epstein and A. V. Olinto, Ultrahigh energy cosmic rays from young neutron star winds, Astrophys. J. **533**, L123 (2000) doi:10.1086/312626 [astro-ph/9912240].

[101] K. Kotera, E. Amato and P. Blasi, The fate of ultrahigh energy nuclei in the immediate environment of young fast-rotating pulsars, JCAP **1508**, no. 08, 026 (2015) doi:10.1088/1475-7516/2015/08/026 [arXiv:1503.07907 [astro-ph.HE]].

[102] Y. P. Ochelkov and V. V. Usov, Curvature radiation of relativistic particles in the magnetosphere of pulsars Astrophys. Space Sci. **69**, 439 (1980) doi:10.1007/BF00661929.

[103] A. Levinson, Particle acceleration and curvature TeV emission by rotating supermassive black holes, Phys. Rev. Lett. **85**, 912 (2000). doi:10.1103/PhysRevLett.85.912 [hep-ph/0002020].

[104] A. Levinson and E. Boldt, UHECR production by a compact black hole dynamo: Application to Sgr A*, Astropart. Phys. **16**, 265 (2002). doi:10.1016/S0927-6505(01)00116-5 [astro-ph/0012314].

[105] D. Whysong and R. Antonucci, Thermal emission as a test for hidden nuclei in nearby radio galaxies, Astrophys. J. **602**, 116 (2004) doi:10.1086/380828 [astro-ph/0207385].

[106] K. Meisenheimer *et al.*, Resolving the innermost parsec of Centaurus A at mid-infrared wavelengths, Astron. Astrophys. **471**, 453 (2007) doi:10.1051/0004-6361:20066967 [arXiv:0707.0177 [astro-ph]].

[107] https://ned.ipac.caltech.edu.

[108] T. Wiklind and C. Henkel, Cold dust in elliptical galaxies Astron. Astrophys. **297**, L71 (1995).

[109] M. Joy, D. F. Lester, P. H. Harvey and H. B. Ellis, The origing of the infrared luminosity in Centaurus A Astrophys. J. **326**, 662 (1988).

[110] A. Eckart, M. Cameron, H. Rothermel, W. Wild, H. Zinnecker, G. Rydbeck, M. Olberg and T. Wiklind, Observations of CO isotopic emission and the far-infrared continuum of Centaurus A Astrophys. J. **363**, 451 (1990).

[111] W. Wild and A. Eckart, Dense gas in the dust lane of Centaurus A, Astron. Astrophys. **359**, 483 (2000) [astro-ph/0005401].

[112] L. Stawarz, F. Aharonian, S. Wagner and M. Ostrowski, Absorption of nuclear gamma-rays on the starlight radiation in FR I sources: the case of Centaurus A, Mon. Not. Roy. Astron. Soc. **371**, 1705 (2006) doi:10.1111/j.1365-2966.2006.10807.x [astro-ph/0605721].

[113] J. A. Graham and R. M. Price, The gaseous filaments in the northeast halo region of NGC 5128 (Centaurus A) Astrophys. J. **247**, 813 (1981).

[114] A. F. Crocker, M. Bureau, L. M. Young and F. Combes, The molecular polar disc in NGC 2768, Mon. Not. Roy. Astron. Soc. **386**, 1811 (2008) doi:10.1111/j.1365-2966.2008.13177.x [arXiv:0803.0426 [astro-ph]].

[115] P. Temi, F. Brighenti and W. G. Mathews, Spitzer observations of passive and star forming early-type galaxies: an infrared color-color sequence, Astrophys. J. **707**, 890 (2009) doi:10.1088/0004-637X/707/2/890 [arXiv:0911.0720 [astro-ph.CO]].

[116] M. J. I. Brown, B. T. Jannuzi, D. J. E. Floyd and J. R. Mould, The ubiquitous radio continuum emission from the most massive early-type galaxies, Astrophys. J. **731**, L41 (2011) doi:10.1088/2041-8205/731/2/L41 [arXiv:1103.2828 [astro-ph.CO]].

[117] P. Temi, F. Brighenti, W. G. Mathews and J. D. Bregman, Cold dust in early-type galaxies I: Observations, Astrophys. J. Suppl. **151**, 237 (2004) doi:10.1086/381963 [astro-ph/0312248].

[118] C. Patrignani *et al.* [Particle Data Group], Review of Particle Physics, Chin. Phys. C **40**, no. 10, 100001 (2016). doi:10.1088/1674-1137/40/10/100001

[119] A. Marconi, G. Pastorini, F. Pacini, D. J. Axon, A. Capetti, D. Macchetto, A. M. Koekemoer and E. J. Schreier, The supermassive black hole in Centaurus A: A benchmark for gas kinematical measurements, Astron. Astrophys. **448**, 921 (2006) doi:10.1051/0004-6361:20053853 [astro-ph/0507435].

[120] N. Neumayer, M. Cappellari, J. Reunanen, H. W. Rix, P. P. van der Werf, P. T. de Zeeuw and R. I. Davies, The central parsecs of Centaurus A: high excitation gas, a molecular disk, and the mass of the black hole, Astrophys. J. **671**, 1329 (2007) doi:10.1086/523039 [arXiv:0709.1877 [astro-ph]].

[121] M. Cappellari, N. Neumayer, J. Reunanen, P. P. van der Werf, P. T. de Zeeuw and H.-W. Rix, The mass of the black hole in Centaurus A from SINFONI AO-assisted integral-field observations of stellar kinematics, Mon. Not. Roy. Astron. Soc. **394**, 660 (2009) doi:10.1111/j.1365-2966.2008.14377.x [arXiv:0812.1000 [astro-ph]].

[122] F. W. Stecker, Photodisintegration of ultrahigh-energy cosmic rays by the universal radiation field, Phys. Rev. **180**, 1264 (1969). doi:10.1103/PhysRev.180.1264

[123] L. A. Anchordoqui, J. F. Beacom, H. Goldberg, S. Palomares-Ruiz and T. J. Weiler, TeV γ-rays and neutrinos from photodisintegration of nuclei in Cygnus OB2, Phys. Rev. D **75**, 063001 (2007) doi:10.1103/PhysRevD.75.063001 [astro-ph/0611581].

[124] S. Karakula and W. Tkaczyk, The formation of the cosmic ray energy spectrum by a photon field, Astropart. Phys. **1**, 229 (1993). doi:10.1016/0927-6505(93)90023-7

[125] P. L. Biermann and P. A. Strittmatter, Synchrotron emission from shock waves in active galactic nuclei, Astrophys. J. **322**, 643 (1987). doi:10.1086/165759

[126] J. P. Rachen and P. L. Biermann, Extragalactic ultrahigh-energy cosmic rays I: Contribution from hot spots in FR-II radio galaxies, Astron. Astrophys. **272**, 161 (1993) [astro-ph/9301010].

[127] F. M. Rieger, Cen A as gamma- and UHE cosmic-ray source, Mem. Soc. Ast. It. **83**, 127 (2012) [arXiv:1108.4565 [astro-ph.HE]].

[128] L. A. Anchordoqui, J. F. Beacom, H. Goldberg, S. Palomares-Ruiz and T. J. Weiler, TeV gamma-rays from photo-disintegration/de-excitation of cosmic-ray nuclei, Phys. Rev. Lett. **98**, 121101 (2007) doi:10.1103/PhysRevLett.98.121101 [astro-ph/0611580].

[129] R. S. Nemmen, C. Bonatto and T. Storchi-Bergmann, A correlation between the highest energy cosmic rays and nearby active galactic nuclei detected by Fermi, Astrophys. J. **722**, 281 (2010) doi:10.1088/0004-637X/722/1/281 [arXiv:1007.5317 [astro-ph.HE]].